Optimal multi-epoch combination of direct imaging observations for improved exoplanet detection

Jules Dallant, Maud Langlois, Éric Thiébaut, Olivier Flasseur

Optimal multi-epoch combination of direct imaging observations for improved exoplanet detection

Jules Dallant[a], Maud Langlois[a], Éric Thiébaut[a], and Olivier Flasseur[b]

[a]CRAL, CNRS, Université de Lyon, ENS, 9 avenue Charles André, 69561 Saint-Genis-Laval Cedex, France
[b]LESIA, Observatoire de Paris, Université PSL, CNRS, Sorbonne Université, Université de Paris, 5 place Jules Janssen, F-92190 Meudon, France

ABSTRACT

Exoplanets detection by direct imaging remains one of the most challenging field of modern astronomy. The signal of the star can prevent the detection of orbiting companions in single datasets, but combining information from several observations helps boost the detection limits. We propose a new algorithm named PACOME, based on PACO's approach, which optimally combines, in a maximum likelihood sense, multi-epoch datasets and improves the detection sensitivity of potential exoplanets by taking into account their orbital motions. The efficiency of the algorithm is tested on the well-known exoplanetary system 51 Eridani.

Keywords: direct imaging, high-contrast, exoplanets, multi-epoch observations, Keplerian motion, optimization, maximum likelihood estimation

1. INTRODUCTION

High-contrast direct imaging is an observational technique particularly adapted to the study of young and massive planets. Despite its interest, only a small number of exoplanets have been detected so far due to the very high contrast between the signal of the star and the one of the planet (10^4 to 10^8).

Signal and image processing methods are therefore systematically applied to the data to reduce the nuisance of residual stellar leakages plus noise (despite attenuation by a coronagraph) and to ease the detection of exoplanetary companions orbiting close to their star. The most common methods are based on Angular Differential Imaging (ADI) and Angular Spectral Differential Imaging (ASDI) which make use of the rotation imposed on the field of view during the observation sequence (and/or the spectral variety of the data) to cancel out the contribution of stellar leakages.

Among the new data processing techniques recently developed is the PACO algorithm.[1] It learns locally the statistics of the nuisance (stellar contamination and noise) including the spatial and spectral correlations within the ADI or ASDI data at each epoch of observation to detect faint sources in the field.

We present in this proceeding the key ingredients of a new method named PACOME (PACO Multi-Epoch) which combines optimally the signal of interest of ADI data from several epochs by maximizing the likelihood of the data based on the supposed orbital motion of potential exoplanets. The proposed method will be described in further details in a paper currently in preparation.

2. THE PACOME ALGORITHM

Our approach is based on the combination of multi-epoch ADI direct imaging observations assuming the Keplerian motion of the searched exoplanets[2] and integrates PACO's unique detection formalism. We derive a criterion that allows to optimally combine ADI observations from different epochs by maximizing the likelihood of the observations given our model.

Further author information: Send correspondence to jules.dallant@univ-lyon1.fr

2.1 Mathematical formalism

Classical ADI data are sequences of coronagraphic images, decoupled into multiple spectral channels recorded at given observation times t. The apparent position on the sky $\boldsymbol{\theta}_t(\boldsymbol{\mu})$ of a celestial body following a Keplerian motion depends on seven orbital elements that we want to estimate (denoted by $\boldsymbol{\mu}$) and on the epoch t of observations.

We model the data $r_{t,\ell,k}$ at epoch t, spectral channel ℓ and frame k as:[3]

$$r_{t,\ell,k} = \alpha_{t,\ell}\, h_{t,\ell,k}(\boldsymbol{\theta}_t(\boldsymbol{\mu})) + f_{t,\ell,k}\,, \tag{1}$$

with $\alpha_{t,\ell} \geq 0$ the source flux assumed identical at all frames of a same epoch ($\alpha_{t,\ell} = 0$ in the absence of such source), $h_{t,\ell,k}(\boldsymbol{\theta}_t(\boldsymbol{\mu}))$ the off-axis PSF of the source at position $\boldsymbol{\theta}_t(\boldsymbol{\mu})$, and $f_{t,\ell,k}$ the nuisance term accounting for stellar leakages and noise.

The flux collected at each pixel of the detector is sufficient to approximate the statistics of the nuisance term by a multivariate Gaussian whose expectation is independent of the frame, i.e. $f_{t,\ell,k} \sim \mathcal{N}(\bar{f}_{t,\ell}, \Sigma_{t,\ell,k})$.[1] The log-likelihood of the data given the model at epoch t, spectral channel ℓ and frame k then writes:

$$\mathcal{L}_{t,\ell,k}(\alpha_{t,\ell}, \boldsymbol{\mu}) = \log p(r_{t,\ell,k} |\, \alpha_{t,\ell}, \boldsymbol{\mu}) = \text{cste} - \frac{1}{2} \left\| r_{t,\ell,k} - \alpha_{t,\ell}\, h_{t,\ell,k}(\boldsymbol{\theta}_t(\boldsymbol{\mu})) - \bar{f}_{t,\ell} \right\|^2_{\mathrm{W}_{t,\ell,k}}, \tag{2}$$

with $\mathrm{W}_{t,\ell,k} = \Sigma^{-1}_{t,\ell,k}$ the precision matrix. For epoch t and spectral channel ℓ, the log-likelihood is equal to:

$$\begin{aligned}
\mathcal{L}_{t,\ell}(\alpha_{t,\ell}, \boldsymbol{\mu}) &= \sum\nolimits_k \mathcal{L}_{t,\ell,k}(\alpha_{t,\ell}, \boldsymbol{\mu}) \\
&= \text{cste} - \frac{1}{2} \sum\nolimits_k \left\| r_{t,\ell,k} - \alpha_{t,\ell}\, h_{t,\ell,k}(\boldsymbol{\theta}_t(\boldsymbol{\mu})) - \bar{f}_{t,\ell} \right\|^2_{\mathrm{W}_{t,\ell,k}} \\
&= \text{cste} + \alpha_{t,\ell}\, b_{t,\ell}(\boldsymbol{\theta}_t(\boldsymbol{\mu})) - \frac{1}{2} \alpha^2_{t,\ell}\, a_{t,\ell}(\boldsymbol{\theta}_t(\boldsymbol{\mu}))\,,
\end{aligned} \tag{3}$$

where $a_{t,\ell}$ and $b_{t,\ell}$ represent respectively a normalization term and the centered and whitened data correlated with the whitened shape of the signal of interest. Both terms are pre-calculated by the PACO algorithm in small local patches as:

$$a_{t,\ell}(\boldsymbol{\theta}_t(\boldsymbol{\mu})) = \sum\nolimits_k h_{t,\ell,k}(\boldsymbol{\theta}_t(\boldsymbol{\mu}))^{\mathrm{t}}\, \mathrm{W}_{t,\ell,k}\, h_{t,\ell,k}(\boldsymbol{\theta}_t(\boldsymbol{\mu}))\,, \tag{4}$$

$$b_{t,\ell}(\boldsymbol{\theta}_t(\boldsymbol{\mu})) = \sum\nolimits_k h_{t,\ell,k}(\boldsymbol{\theta}_t(\boldsymbol{\mu}))^{\mathrm{t}}\, \mathrm{W}_{t,\ell,k}\, (r_{t,\ell,k} - \bar{f}_{t,\ell}). \tag{5}$$

The epochs t are independent as well, the $r_{t,\ell,k}$ term is centered by the estimated temporal mean $\bar{f}_{t,\ell}$ and spatially whitened by the precision matrix $\mathrm{W}_{t,\ell,k}$. We can therefore establish, for spectral channel ℓ, the total log-likelihood of the data:

$$\mathcal{L}_\ell(\boldsymbol{\alpha}, \boldsymbol{\mu}) = \sum_t \mathcal{L}_{t,\ell}(\alpha_{t,\ell}, \boldsymbol{\mu}). \tag{6}$$

The source flux estimator (in the maximum likelihood sense) has a closed-form expression which is expressed as a function of the previous pre-calculated $a_{t,\ell}$ and $b_{t,\ell}$ terms:

$$\widehat{\alpha}_{t,\ell} = \underset{\alpha_{t,\ell} \geq 0}{\arg\max}\ \mathcal{L}_{t,\ell}(\alpha_{t,\ell}, \boldsymbol{\mu}) = \frac{\left[b_{t,\ell}(\boldsymbol{\theta}_t(\boldsymbol{\mu})) \right]_+}{a_{t,\ell}(\boldsymbol{\theta}_t(\boldsymbol{\mu}))}\,, \tag{7}$$

where $[\cdot]_+$ denotes the argument's positive part taken term by term. By injecting the source flux estimators in $\mathcal{L}_\ell(\boldsymbol{\alpha}, \boldsymbol{\mu})$, it is possible to express the log-likelihood as being only dependent on the orbital elements $\boldsymbol{\mu}$:

$$\mathcal{L}_\ell(\boldsymbol{\mu}) = \text{cste} + \frac{1}{2} \sum_t \frac{\left[b_{t,\ell}(\boldsymbol{\theta}_t(\boldsymbol{\mu})) \right]^2_+}{a_{t,\ell}(\boldsymbol{\theta}_t(\boldsymbol{\mu}))}. \tag{8}$$

Finally, the optimal orbital elements, in the maximum likelihood sense, satisfy:

$$\widehat{\boldsymbol{\mu}}_\ell = \arg\max_{\boldsymbol{\mu}} \sum_t \frac{\left[b_{t,\ell}(\boldsymbol{\theta}_t(\boldsymbol{\mu}))\right]_+^2}{a_{t,\ell}(\boldsymbol{\theta}_t(\boldsymbol{\mu}))}. \tag{9}$$

Having no analytic expression, the optimal orbital elements $\widehat{\boldsymbol{\mu}}$ are only accessible through the use of global optimization numerical methods. Hence, our problem amounts to optimize the following multi-epoch objective function:

$$\mathcal{C}_\ell(\boldsymbol{\mu}) = \sum_t \frac{\left[b_{t,\ell}(\boldsymbol{\theta}_t(\boldsymbol{\mu}))\right]_+^2}{a_{t,\ell}(\boldsymbol{\theta}_t(\boldsymbol{\mu}))}. \tag{10}$$

The criterion $\mathcal{C}_\ell(\boldsymbol{\mu})$ of Equation (10) combines optimally the information within the data and should enable the detection of sources yet undetectable in individual epochs and simultaneously provide an estimation of their orbital elements.

2.2 Implementation of the algorithm

The PACOME algorithm proceeds by sampling the criterion $\mathcal{C}_\ell(\boldsymbol{\mu})$ of Equation (10) on a 7-D regularly-spaced grid followed by a local optimization refinement. The main steps of the algorithm are summarized in Figure 1.

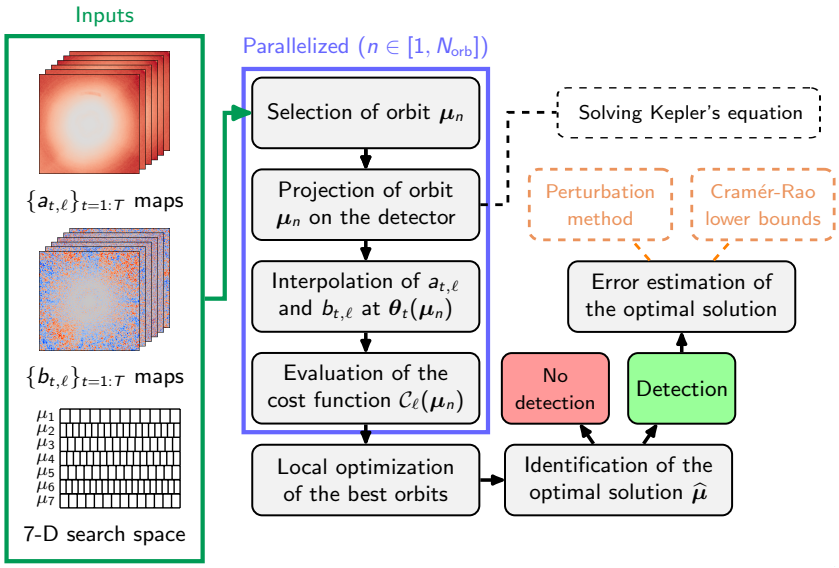

Figure 1. Main steps of the PACOME algorithm.

The dimensionality of the problem and the presence of noise in the data causes the criterion to behave erratically on local scales. Therefore we perform an exhaustive search of the potential optimal solution on a regular 7-D grid. This approach is costly but necessary to approach as close as possible the global maximum of the criterion.

For each orbit of the grid, we compute its 2-D projected position on the detector at all epochs. Each projected positions calculation requires solving Kepler's equation which has no analytical solution but can be solved with root-finding numerical methods such as Brent's[4] `fzero` algorithm.

Since the projected positions are arbitrary, they have a finer resolution than the detector's pixel grid and therefore than the $a_{t,\ell}$ and $b_{t,\ell}$ maps provided by PACO. To deal with this resolution problem, we interpolate the maps $a_{t,\ell}$ and $b_{t,\ell}$. The choice of the interpolation method is quite critical. We compared several interpolation functions, including the Lanczos four-neighbor interpolation function,[5] which is the best suited to our problem

by giving higher criterion values. The Catmull-Rom spline interpolation[5] also proved to be almost as efficient while being slightly faster.

After interpolating the $a_{t,\ell}$ and $b_{t,\ell}$ values at the projected positions of all epochs, the objective function is evaluated given Equation 10.

The N best on-grid orbits having the highest criterion values (among the total $N_{\rm orb}$ explored orbits) are selected and their orbital elements are locally refined via an numerical optimization algorithm maximizing the cost function. For this, we use the VMLMB optimization method,[6] which is a memory limited quasi-Newton method with bound constraints. The gradient of the objective function is computed by finite differences.

The finest of the N best refined orbits is finally retained as the optimal multi-epoch solution $\widehat{\boldsymbol{\mu}}$. We compute a $5\sigma_{\mathcal{C}}$ multi-epoch detection limit from the empirical distribution of the criterion when combined with pure noise. The cost value of the optimal solution is compared to the $5\sigma_{\mathcal{C}}$ limit to decide or not on a detection.

If the cost function is at least five times the noise limit, a detection is claimed and the error associated to the optimal orbital elements are estimated by one of the two methods we have implemented. The first one is a perturbative method which consists in injecting repeatedly in the data random realizations of Gaussian noise of the same order of magnitude as the signal variance. The solution is re-optimized on the perturbed data in order to empirically estimate the standard deviation of the optimal orbital elements. The second method is analytical and exploits the Cramér-Rao bounds.[7] It is faster than the first one but sensitive to possible orbital elements degeneracies since it requires to invert an estimate of the Fisher information matrix.

3. APPLICATION TO THE 51 ERIDANI SYSTEM

3.1 Observations description and setup of the search

We demonstrate the efficiency of our method on the star 51 Eridani hosting one giant planet known as 51 Eridani b discovered by the Gemini Planet Imager (GPI).[8] The study is performed on 6 Angular Differential Imaging datasets lasting around 7 hours of observation time and spanning over 4 years obtained with the VLT/SPHERE-IRDIS[9] in K1-K2 and H2-H3 dual bands. A summary of the data used with the algorithm is given in Table 1. The $a_{t,\ell}$ and $b_{t,\ell}$ maps were pre-computed beforehand by the PACO algorithm for each epoch and spectral channel. These terms were interpolated during PACOME's search with the Catmull-Rom (cubic Hermite) spline for faster computation. The planet flux being higher in K1 and H2 bands, we chose the first spectral channel of all epochs for the rest of this study ($\ell = 1$).

Table 1. IRDIS observations of 51 Eridani used in this paper.

UT date	**MJD**	**Bands**	$\mathbf{N_{frames}}$	$\mathbf{t_{exp}}$ (s)
2015-09-25	57290.3947546	K1-K2	256	16
2015-12-26	57382.1254652	H2-H3	256	16
2016-01-16	57403.0951110	H2-H3	256	16
2016-12-13	57735.1723974	H2-H3	72	64
2017-09-28	58024.3851123	K1-K2	192	24
2019-11-28	58815.2493445	K1-K2	180	24

The orbital elements search space is given in Table 2. It is deliberately chosen to cover a wide field of view encompassing the known exoplanet 51 Eri b. The objective function of Equation (10) was evaluated for $\sim 51\times10^9$ orbits in total and the computation took about 10 hours of CPU time on 12 cores with a code written in Julia.[10] We re-optimized the orbital elements of the first best $N = 1000$ orbits. The finest of them all was kept and is presented in section 3.2.

3.2 Results of the search

The optimal solution $\widehat{\boldsymbol{\mu}}$ found by PACOME has a score of $\mathcal{C}(\widehat{\boldsymbol{\mu}}) = 760.68 \sim 80\sigma_{\mathcal{C}}$ which is largely above the standard 5σ detection confidence required to claim a detection. The associated 2-D projected positions $\boldsymbol{\theta}_t(\widehat{\boldsymbol{\mu}})$ correspond to the positions of the known companion 51 Eri b[8,11] The values of the optimal orbit and their associated errors (estimated with the empirical perturbation method) are displayed in Table 3 and compared to

Table 2. Orbital elements search space of the PACOME run on 51 Eridani.

Name	Symbol	Unit	Min val.	Max val.	N_{points}
Semi-major axis	a	mas	200	600	25
Eccentricity	e	-	0	0.6	13
Inclination	i	deg	0	180	50
Epoch of periapsis passage	τ	-	0	1	50
Argument of periapsis	ω	deg	0	360	50
Longitude of ascending node	Ω	deg	0	360	50
Kepler's constant	K	mas^3/yr^2	63503	67353	25

the ones obtained in Maire et al. 2019.[12] We converted our orbital elements into the units used in Maire et al. to ease the comparison by using Gaia's estimation of the parallax $\pi = 33.4390 \pm 0.0777$.

Our results agree with theirs within the error bars except for the semi-major axis a which seems to be estimated slightly larger by our method. Our eccentricity is also a bit larger which could justify the semi-major axis stretching out to reach the same 2-D positions. Kepler's constant, and therefore the stellar mass, is a free parameter in our algorithm. Our solution yields $M_\star = 1.72 \pm 0.014 M_\odot$ which also agrees with the literature ($M_\star = 1.75 \pm 0.05 M_\odot$).

It is worth noticing that the orbital solution of Maire et al. 2019[12] was computed on 10 astrometric measurements (6 SPHERE and 4 GPI) with the orbit fitting Bayesian rejection-sampling method `OFTI`[13] whereas 6 observations were used in this work, which could explain the slight difference we note.

Table 3. Optimal orbital elements $\widehat{\boldsymbol{\mu}}$ found with PACOME for 51 Eri b

Elem.	Unit	This work	Maire et al. 2019
a	au	$17.94^{\pm 0.63}$	12^{+4}_{-2}
e	-	$0.54^{\pm 0.05}$	$0.45^{+0.10}_{-0.15}$
i	deg	$126.57^{\pm 3.21}$	133^{+14}_{-7}
τ	yr	$2025.72^{\pm 19.0}$	2011^{+16}_{-5}
ω	deg	$67.6^{\pm 6.72}$	87^{+34}_{-30}
Ω	deg	$124.27^{\pm 9.87}$	103^{+53}_{-90}
K	mas^3/yr^2	64305.08 ± 301.52	-
P	yr	$57.93^{\pm 3.07}$	32^{+17}_{-9}
$\mathcal{C}$		760.68	-
$5\sigma_{\mathcal{C}}$		49.49	-

51 Eridani b is not detected in all individual epochs with IRDIS. Indeed, in 2 of the 6 epochs the signal-to-noise ratio (SNR) of the source is below the 5σ detection limit (i.e. SNR ≥ 5) and one is at the very limit with an SNR value of 5.3. Yet PACOME still manages to find the source signal in these epochs as illustrated on Figure 2. The individual SNR maps centered around the 2-D projected positions of the optimal solution at each epoch are plotted in Figure 2. For comparison, we plot the 2-D map of the criterion centered around the optimal solution on Figure 3 which clearly shows that the signal combines very efficiently and the noise all around the solution follows a statistical distribution incompatible with planet detection. The 2-D map is re-sampled by a factor 4 using the interpolation function described in section 3.1.

Finally, the projection of the optimal orbit found by PACOME is shown in Figure 4 along with all other explored orbits having criterion scores $\mathcal{C}$ higher than 700 (7486 orbits in total). In this figure, two families of probable orbits seem to emerge: the first is elongated along the ascending declination direction and the other one (similar to the retained solution) slightly inclined towards the descending right ascension direction. This can be explained by the small temporal coverage of the data which only spans over a small portion of the recovered orbit. It is thus very poorly constrained and it allows other orbits to pass through the same 2-D projected positions and still get high criterion values.

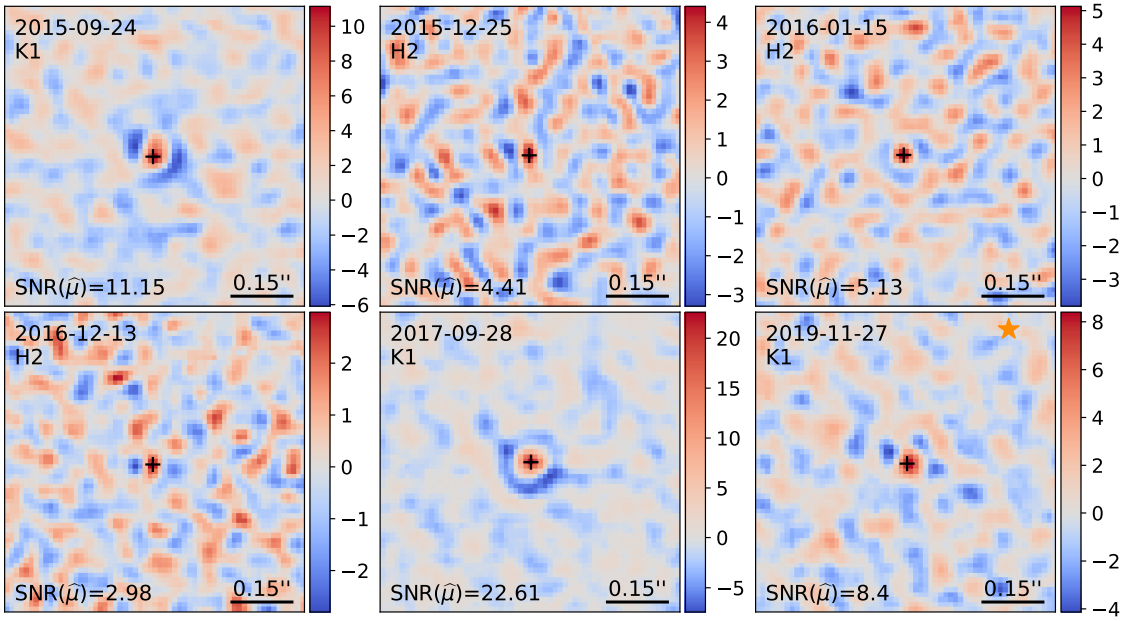

Figure 2. Individual $\mathrm{SNR}_{t,\ell} = \dfrac{b_{t,\ell}}{\sqrt{a_{t,\ell}}}$ maps around the best solution $\widehat{\boldsymbol{\mu}}$. The black cross indicates the exoplanet location found by PACOME.

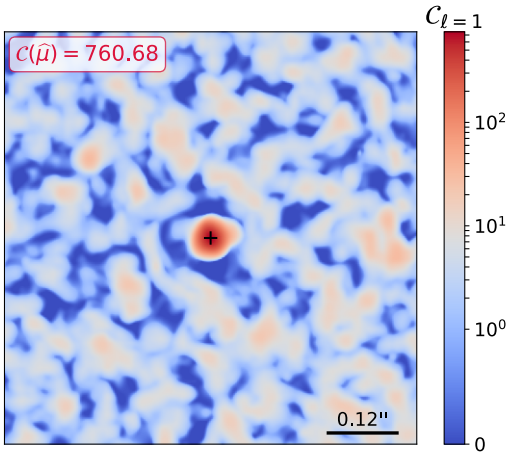

Figure 3. Cost function map around the optimal solution $\widehat{\boldsymbol{\mu}}$ sampled with 4 nodes per pixel.

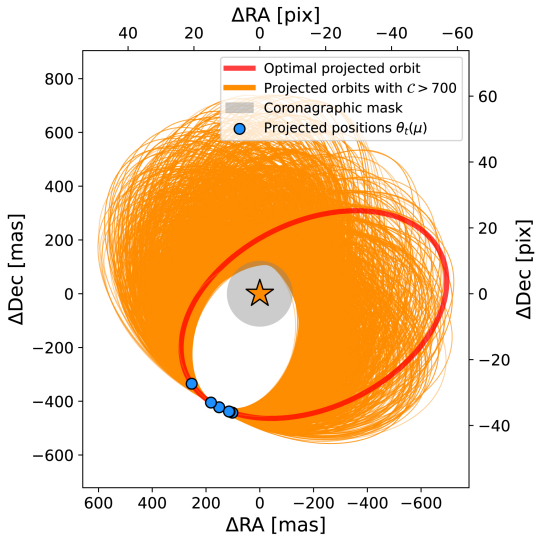

Figure 4. Optimal orbit $\widehat{\boldsymbol{\mu}}$ (red) and all the other best orbits with $\mathcal{C} > 700$ (orange).

4. CONCLUSION

We developed a method which allows, by computing an optimal criterion of multi-epoch combination, to detect exoplanets and to estimate precisely their orbital parameters simultaneously. It is optimal in the maximum likelihood sense, it benefits from the high sensitivity of the PACO algorithm and it is faster than other multi-epoch combination algorithms[2] which take several weeks of computation time on GPU as opposed to a few hours on CPU for our method.

Applying the method to the 51 Eridani system allowed to find the orbit of the known planet, compatible with the literature. The method is designed to increase the detection capability but it did not lead to the detection of a new planet in theses datasets.

We consider several developments for the algorithm. Using our method with PACO-processed ASDI data,[14] capturing the spectral and temporal fluctuations of the nuisance and thus reducing detection artifacts, will allow to further increase the detection limit and eventually detect new exoplanets. A smarter on-search grid refinement sampling strategy will be explored for better computation efficiency and to ensure that the global maximum of the criterion is not missed. The detection benefits of a possible flux-wise data calibration will be studied. Finally, the gain in contrast achieved by the method will be quantified by simulating synthetic sources at different levels of fluxes in the data and other promising exoplanetary systems will be probed. Most of these developments will be described in more detail in a paper in preparation (Dallant et al.).

ACKNOWLEDGMENTS

This work was supported by the Programme National de Planétologie (PNP) and the Action Spécifique Haute Résolution Angulaire (ASHRA) of CNRS/INSU co-funded by CNES.

REFERENCES

[1] Flasseur et al., "Exoplanet detection in angular differential imaging by statistical learning of the nonstationary patch covariances - The PACO algorithm," *A&A* **618**, p. A138, 2018.

[2] Nowak et al., "K-Stacker: Keplerian image recombination for the direct detection of exoplanets," *A&A* **615**, p. A144, 2018.

[3] Thiébaut et al., "Fast and robust exo-planet detection in multi-spectral, multi-temporal data," in *Adaptive Optics Systems V*, E. Marchetti, L. M. Close, and J.-P. Véran, eds., **9909**, pp. 1534 – 1543, International Society for Optics and Photonics, SPIE, 2016.

[4] R. Brent, *Algorithms for Minimization without Derivatives*, Englewood Cliffs, NJ: Prentice-Hall, 1973.

[5] W. Burger and M. J. Burge, *Principles of Digital Image Processing*, Springer London, 2009.

[6] E. Thiébaut, "Optimization issues in blind deconvolution algorithms," in *Astronomical Data Analysis II*, J.-L. Starck and F. D. Murtagh, eds., **4847**, pp. 174–183, SPIE, (Bellingham, Washington), 2002.

[7] S. M. Kay, *Fundamentals of Statistical Signal Processing: Estimation Theory*, vol. 1, Prentice Hall, 1997.

[8] Macintosh et al., "Discovery and spectroscopy of the young jovian planet 51 Eri b with the Gemini Planet Imager," *Science* **350**(6256), pp. 64–67, 2015.

[9] Beuzit et al., "SPHERE: the exoplanet imager for the Very Large Telescope," *A&A* **631**, p. A155, 2019.

[10] Bezanson et al., "Julia: A Fresh Approach to Numerical Computing," *SIAM Review* **59**(1), pp. 65–98, 2017.

[11] Samland et al., "Spectral and atmospheric characterization of 51 Eridani b using VLT/SPHERE," *A&A* **603**, p. A57, 2017.

[12] Maire et al., "Hint of curvature in the orbital motion of the exoplanet 51 Eridani b using 3 yr of VLT/SPHERE monitoring," *A&A* **624**, p. A118, 2019.

[13] Blunt et al., "Orbits for the impatient: A bayesian rejection-sampling method for quickly fitting the orbits of long-period exoplanets," *The Astronomical Journal* **153**, p. 229, apr 2017.

[14] Flasseur et al., "PACO ASDI: an algorithm for exoplanet detection and characterization in direct imaging with integral field spectrographs," *A&A* **637**, p. A9, 2020.